





A Low-Noise Amplifier in Submicron CMOS for Neural Recording on Optogenetics Applications

H. E. Oshiro^{1,2}^a, R. A. P. Andrade²^b, J. N. S. Junior¹^c, M. Luppe¹^d,
E. Colombari³^e, M. C. Dias⁴^f and J. P. Carmo¹^g

¹Group of Metamaterials Microwaves and Optics (GMeta), Department of Electrical Engineering (SEL), University of São Paulo (USP), Avenida Trabalhador São-Carlense, Nr. 400, São Carlos 13566-590, SP, Brazil

²brain4care, Avenida Bruno Ruggiero Filho, 971 - Parque Santa Felícia Jardim, São Carlos, SP, 13562-420, Brazil

³Department of Physiology and Pathology, Faculty of Odontology, São Paulo State University (UNESP), Rua Humaitá, Nr. 1680, Araraquara 14801-385, SP, Brazil

⁴Faculty of Medicine, University of Porto, Alameda Hernani Monteiro, piso 8, Unidade Cuidados Neurocriticos, 4200-319, Porto, Portugal


Keywords: Low-Noise Amplifier, Bioamplifier, CMOS, Optogenetics, Neuronal Signal.


Abstract: Optogenetics combines optical and genetic techniques to control and monitor neuronal activities. Recent efforts seek the development of portable and even wireless electronics for optical activation and acquisition of biopotentials, aiming to offer greater mobility and freedom to study animals, in contrast to the large equipment commonly found in laboratories that perform the activation of lasers, signal amplifiers and acquisition. In this context, this paper reports on the design and simulation of a low-noise amplifier (LNA) to acquire neural signals on optogenetics applications. The simulations showed that with the nominal voltage supply of 1.8V this LNA is able to amplify neuronal signals in the range of 0.3Hz up to ≈ 172 kHz with a gain of ≈ 39.3 dB, while rejecting DC offsets generated at the interface between the electrodes. The simulations also showed that with variations of $\pm 20\%$ with relation to the nominal voltage supply, the worse cases of the lower and higher cut-off frequencies were 0.3Hz (increased) and 51.3kHz (decreased), respectively. Moreover, under these stressing conditions the gain had a variation between ≈ 36.8 dB for the worst scenario and ≈ 40 dB for the best scenario. These results are more than enough to meet the bandwidth requirements on optogenetics and it can be concluded that the specifications of the LNA are not affected by the useful life of batteries under the aforementioned voltage variation range. The power consumption of the system is around 64μ W from a 1.8V voltage supply. This LNA was designed in the 6-metals/1-poly 0.18 μ m CMOS process from UMC (United Microelectronics Corporation) and occupies an area of 0.092mm².


1 INTRODUCTION


The Optogenetics combines optical and genetic techniques to control and monitor neuronal activities (Deisseroth, 2011). Recent efforts seek the development of portable and even wireless electronics for optical activation and acquisition of


biopotentials, aiming to offer greater mobility and freedom to study animals, in contrast to the large equipment commonly found in laboratories that perform the activation of lasers, signal amplifiers and acquisition. For this reason, the optogenetics is an emergent field of applications, where the signals are acquired from a specific part of the brain and at the


^a <https://orcid.org/0000-0003-0370-4700>

^b <https://orcid.org/0000-0002-7248-4636>

^c <https://orcid.org/0000-0002-1975-2267>

^d <https://orcid.org/0000-0001-7419-2154>

^e <https://orcid.org/0000-0002-1395-4036>

^f <https://orcid.org/0000-0003-0340-9808>

^g <https://orcid.org/0000-0001-7955-7503>

same time this same part can also be stimulated with light and, in this context, Figure 1(a) shows the concept of electrode with a *chip-in-the-tip* for optogenetics, where a bio-amplifier and the respective signal processing/control/interface electronics simultaneously acquires the neuronal signals and stimulates through light. This paper presents the design of a fully integrated bio-amplifier suitable for recording biological signal within the range of 1Hz up to 10kHz that was designed in the 6-metals/1-poly 0.18 μ m CMOS process from the UMC. The simulations showed that these specifications were met for the nominal voltage of 1.8V, even with the LNA stressed with high variations of $\pm 20\%$.

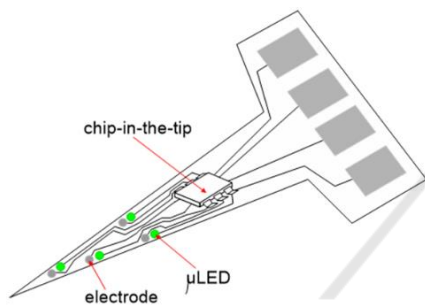


Figure 1: Illustration of the *chip-in-the-tip* concept for application in optogenetics.

2 CIRCUIT DESIGN

2.1 Pseudoresistors and Amplifier Elements

Figure 2 shows the schematic of the proposed LNA, which is composed by an Operational Transconductance Amplifier (OTA) and few discrete passive components. The resistors R_2 are in fact MOS-bipolar devices, where each one is composed by two PMOS transistors connected in series with their bulks and gates connected to the supply rail V_{dd} and their sources tied together. These two pairs of two PMOS form two pseudo-resistors, whose implementation is also depicted in Figure 2 (Harrison *et al.*, 2003) (Wattanapanitch *et al.*, 2007). The pseudoresistors are in the order of T Ω , and they are called ‘pseudo’ because it mimcs the behavior of a real resistor. The parallel of R_2 with C_2 creates a pole in the transfer function (the gain is frequency dependent) with the frequency $f_L = (2\pi R_2 C_2)^{-1}$ with low-pass behaviour. Therefore, R_2 must be in the order of T Ω to compensate for the fact that C_2 is in the order of fF to ensure that f_L

is located as close as possible to the origin and the most as possible smaller than 1Hz that contains neuronal information. This amplifier is also composed by two capacitors ($C_1 \approx 25.8$ pF and $C_2 \approx 206$ fF) and by a transconductance operational amplifier (OTA). In the end, the voltage gain of this amplifier is $A_V = C_1/C_2 = 100 = 40$ dB.

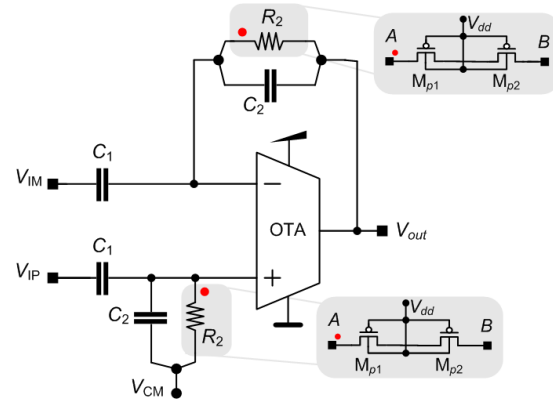


Figure 2: Schematic of the LNA, highlighting the pseudo-resistors components.

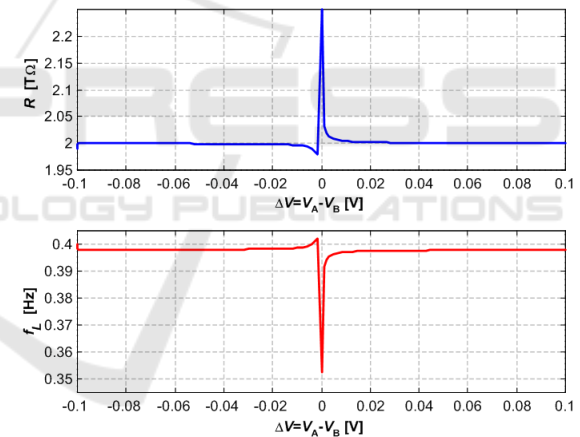


Figure 3: Resistance response of the pseudo-resistors (top plot) and the pole location f_L [Hz] in the transfer function of the LNA (bottom plot) versus the voltage input.

The top plot of Figure 3 shows the simulated resistance response of the pseudo-resistors in terms of the voltage $\Delta V = V_{in} - V_{out}$ at its terminals, where V_{in} is the terminal that connects to the bulk of the first PMOS and V_{out} is the terminal that connects to the gate of last PMOS (in concordance with Figure 2). A voltage pulse source was placed between the V_{in} and V_{out} terminals of the pseudo-resistor, and the voltage were varied between -0.1 V and +0.1 V. The current was simulated obtained, and the resistance was calculated by dividing the voltage by the current. The bottom plot of Figure 3 shows the pole location

f_L [Hz] in the transfer function of the LNA (bottom plot) versus the voltage input. One conclusion comes to light, the lower cut-off frequency f_L more than meets the lower bond specification of the LNA, e.g., $f_L \ll 1$ Hz for any voltage in the range [-0.1,0.1] V.

2.2 Design of the Operational Transconductance Amplifier (OTA)

Figure 4 illustrates the schematic of the OTA, which is composed by eight p-type and six n-type transistors. The output into/from the load capacitor C is given by $I_{out}=g_m \cdot (V^+ - V^-)$, where g_m [S] is the transconductance of the OTA, V^+ corresponds to the positive input (V_{IP}) and V^- to the negative input (V_{IM}) in Figure 2. The circuit of the OTA operates from a 1.8V power supply, and the common mode voltage is set to $V_{CM}=V_{dd}/2=0.9$ V.

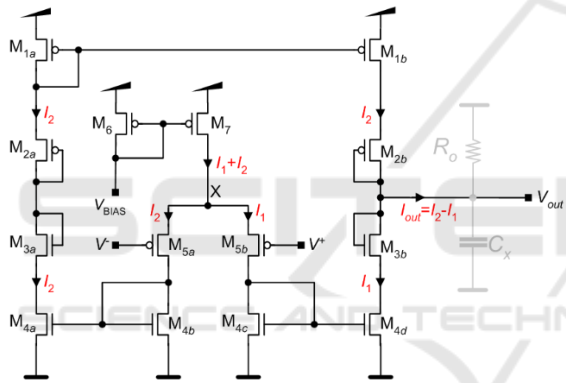


Figure 4: Schematic of the OTA and currents ($I_1=I_2$) for all MOSFETs saturated in strong inversion.

Since $V^+=V_{CM}+in^+$ and $V^-=V_{CM}+in^-$ and $|in^+| \ll V_{CM}$ (frequently, $in^-=-in^+$), thus $V^X \approx \text{constant}$. For $in^+ > in^-$: $I_2 > I_1$. The DC voltage of V_{sg} is the same for M_{1b} and M_{1a} , thus $I_2 > I_1$, forcing:

$$I_{out}=I_2-I_1 > 0 \quad (1)$$

and

$$\Delta V_{out}=(I_{out}/C) \cdot \Delta t > 0 \quad (2)$$

In the opposite situation, for $in^+ < in^-$, the currents are such that:

$$I_{out}=I_2-I_1 < 0 \quad (3)$$

and

$$\Delta V_{out}=(I_{out}/C) \cdot \Delta t < 0 \quad (4)$$

To obtain the output voltage V_{out} in terms of the differential input $\Delta V_{in}=(V^+-V^-)=(in^+-in^-)$, I_1 and I_2 must be obtained. The currents are then:

$$I_1=1/2 \cdot \mu_p C_{ox}(W/L) \cdot (V^+-V_X+V_{thp})^2 \quad (5)$$

with $(W/L)=(W/L)_5$ and

$$I_2=1/2 \cdot \mu_p C_{ox}(W/L) \cdot (V_X-V^-+V_{thp})^2 \quad (6)$$

In this case, the output voltage is given by:

$$V_{out}(\Delta t)=V_0+(I_2-I_1)/C \cdot \Delta t \quad (7)$$

where V_0 is the abstract initial condition/voltage. The signals to amplify are such that $|in^+| \ll V_{CM}$, meaning that:

$$\begin{aligned} V_{out}(\Delta t) &\approx V_0 + [2\mu_p C_{ox}(W/L) \cdot (V_X - V_{CM} + V_{thp}) \times \\ &\quad \times (in^- - in^+) / C] \times \Delta t = \\ &= V_0 - [2\mu_p C_{ox}(W/L) \cdot (V_X - V_{CM} + V_{thp}) / C] \times \\ &\quad \times \Delta V_{in} \times \Delta t \end{aligned} \quad (8)$$

The voltage variation $\Delta V_{out}=V_{out}(\Delta t)-V_0$ in terms of the voltage $\Delta V_{in}=in^+-in^-$ is given by:

$$\begin{aligned} \Delta V_{out} &= 2\mu_p C_{ox}(W/L) \cdot (V_X - V_{CM} + V_{thp}) \cdot (\Delta t / C) \times \\ &\quad \times (in^+ - in^-) = \\ &= K \cdot (in^+ - in^-) \end{aligned} \quad (9)$$

The equation (9) is true for $\lambda=0$ (without the channel length modulation effect). Nonetheless, even with $\lambda \neq 0$, the equation (9) is still true if R_o is high (in the order of M Ω). This resistance can be tuned according the following equation:

$$\begin{aligned} R_o &= R_{o1} // R_{o2} = \\ &= \{r_{o3b} + r_{o4d} \cdot [1 + g_{m3b} \cdot (1 + \eta) \cdot r_{o3b}]\} // \\ &// \{r_{o2b} + r_{o1b} \cdot [1 + g_{m1b} \cdot (1 + \eta) \cdot r_{o2b}]\} \propto [\text{M}\Omega] \end{aligned} \quad (10)$$

with

$$\begin{cases} r_{o3b} = r_{o4d} = (\lambda_n I_{1,2,DC})^{-1} \\ r_{o1b} = r_{o2b} = (\lambda_p I_{1,2,DC})^{-1} \end{cases} \quad (11)$$

and

$$\begin{cases} g_{m2b} = \sqrt{2\mu_p C_{ox}(W/L)_{2b} \times I_{1,2,DC}} \\ g_{m3b} = \sqrt{2\mu_n C_{ox}(W/L)_{3b} \times I_{1,2,DC}} \end{cases} \quad (12)$$

The transconductance of this OTA is given by:

$$g_m = 2\mu_p C_{ox}(W/L) \cdot (V_X - V_{CM} + V_{thp}) = g_{m5} \quad (13)$$

with

$$g_{m5} = [2\mu_p C_{ox}(W/L) \cdot I_{1,2,DC}]^{1/2} \quad (14)$$

2.3 LNA Behaviour: Transfer Function $H_{LNA}(F)=V_{out}/(V_{IP}-V_{IM})$

The LNA faces several challenges due to the nature of the signals to amplify that are characterized by low-amplitudes and low-frequencies very close to the DC component. These types of amplifiers typically

present a mid-band gain of about 40dB, and as stated before, a bandwidth ranging from the 1Hz to 10kHz. The transfer function $H_{LNA}(f)$ of the LNA is given by:

$$H_{LNA}(s) = -\frac{s.(s - 2\pi f_z)}{(s + 2\pi f_z).(s + 2\pi f_H)} \quad (15)$$

Figure 5 depicts the theoretical Bode diagram of $H_{LNA}(f)$ of the LNA, whose transfer function contains two zeros and two poles.

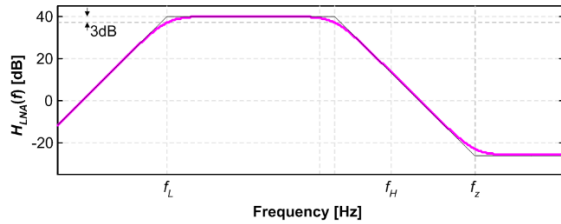


Figure 5: Theoretical Bode diagram of the transfer function $H_{LNA}(f)$ of this LNA.

One zero is located in the origin, while the other is located at $f_z = g_m / (2\pi C_2)$. As stated before, the smallest pole is located in the lower cut-off frequency $f_L = 1 / (2\pi R_2 C_2)$, while the highest pole is located in the upper cut-off frequency $f_H = g_m / (2\pi C_1)$. It must be noted that the frequency of the second zero f_z is much higher than the frequency of any pole. As expected, the LNA gain between f_L and f_H can be determined and as already known, it is approximately given by (C_1 / C_2) . Table 1 lists the dimensions of the MOSFETs that comprises the OTA and the pseudo resistors.

Capacitors C_1 and C_2 were implemented with MIMcaps, which use the Metal 6 and Metal 5 layers as the capacitor's plates. The overlap capacitance already include the fringe field and measures $1\text{fF} \cdot \mu\text{m}^{-1}$ (Europractice, 2025). The option of the used technology was the mini@SIC prototyping. This option offers a shallow trench isolation (STI), triple well, aluminium interconnects for all metals, metal 6 as top metal with a thickness of $20\text{k}\text{\AA}$ (e.g., $2\mu\text{m}$) (Europractice, 2025).

3 RESULTS

The simulations done with the nominal voltage supply of 1.8V showed a midband gain of 39.3dB in the range from 0.3Hz to 172kHz. Figure 6 shows the

frequency response. Below 0.3Hz the loss of gain is approximately 3dB.

Table 1: Dimensions of the MOSFETs that comprises the OTA and the pseudo resistors.

MOSFET	Total (W/L)
M _{1a} , M _{1b}	13.4 μm /20 μm
M _{2a} , M _{2b}	20.6 μm /0.28 μm
M _{3a} , M _{3b}	15.4 μm /0.28 μm
M _{4a} , M _{4b} , M _{4c} , M _{4d}	10 μm /20 μm
M _{5a} , M _{5b}	463 μm /0.51 μm
M ₆ , M ₇	2.3 μm /5.1 μm
Pseudo-resistors M _{p1} to M _{p6}	1 μm /1 μm

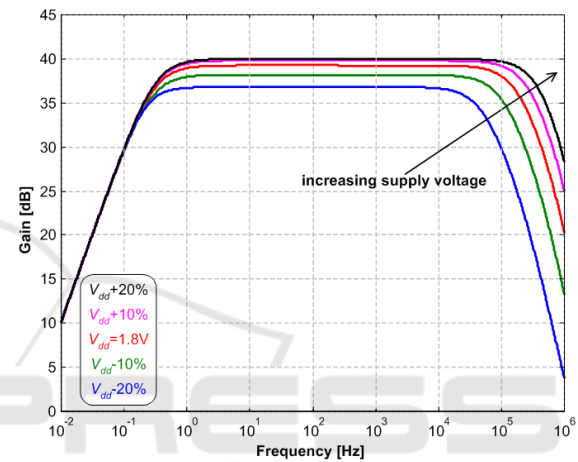


Figure 6: Simulation results with the gain of LNA and respective transfer function $H_{LNA}(f)$.

Few stress tests were applied to the LNA, varying the supply voltage by 10% and 20% in relation to the nominal value. The simulations also showed that the variation in the lower cut-off frequency f_L was not significant but was advantageous, because it reduced from 0.3Hz to 0.2Hz when the supply voltage dropped by 20% in relation to the nominal value. On the other hand, the 20% decrease in supply voltage resulted in the largest reduction in the upper cutoff frequency f_H from 172kHz to 51kHz. In the opposite situation, when the supply voltage increases by 20%, this frequency f_H increases from 172kHz to 355kHz. The gain of LNA varied from 39.3dB to 40dB and 36.8dB, when the supply voltage varied from +20% and -20%, respectively. In resume, the bounds f_L and f_H , as well as, the bandwidth $BW = f_L - f_H$ of the gain are more than enough to cover the range of extracellular recorded spikes from 1Hz to 10kHz. Figure 6 also shows the gains for each stress test.

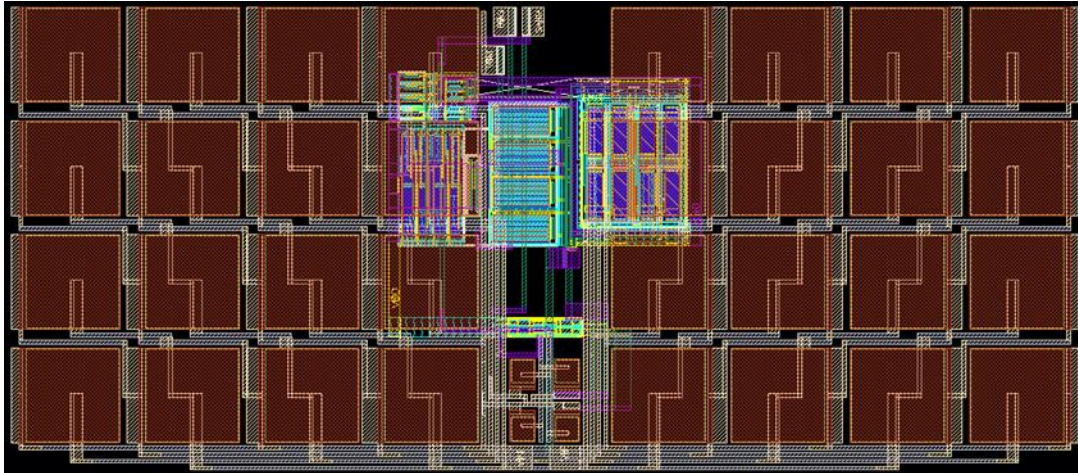


Figure 8: Layout of this LNA.

As illustrated in Figure 7, three different scenarios were also simulated to analyse the robustness of the LNA considering the capacitance and resistance associate to the wires that connect the electrodes to the input of LNA.

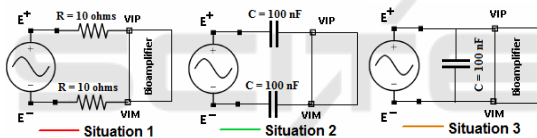


Figure 7: Scenarios for the robustness simulation of LNA.

The resistance was considered around 10Ω in Situation 1. This value is probably higher than the real, but it was an extrapolated value to confirm the previous robustness of the amplifier. The capacitance was considered around 100nF in both Situations 2 and 3. Situation 1 considered a serial resistance existent between the positive electrode E^+ and the positive input of the LNA (V_{IP}), and the one between E^- and V_{IM} . Situation 2 considered a capacitor in series with both positive and negative electrodes. Finally, Situation 3 considered a capacitor placed in parallel to the voltage source.

The three scenarios were simulated for the several voltage supplies described latter. The simulation results revealed that, for a given voltage supply, the gain and the frequencies f_L and f_H were not affected for these parasitics that may be present in the connection wires between the electrodes and the LNA. These results are important because allows to get the conclusion that this LNA is very reliable and robust to external electrical factors on wires.

4 CONCLUSIONS

This paper presented a low-noise amplifier (LNA) that was optimized for use on acquisition of neural signals on optogenetics applications. This LNA is part of a more complete microdevice, comprising optical neurostimulation to meet the need of more compact solutions for research laboratories. Figure 8 shows the layout of the proposed LNA, which occupies an area of silicon of $200\mu\text{m}\times 460\mu\text{m}$.

ACKNOWLEDGEMENTS

This work was partially supported by the CNPq through the project with the reference CNPq 402752/2023-6 and the PQ scholarship with the reference CNPq 305858/2023-8.

REFERENCES

- Deisseroth, K. (2011). Optogenetics, *Nature Methods*, Vol. 8, No. 1, pp. 26-29.
- Harrison, R.R.; Charles, C. (2003). A low-power low-noise cmos for amplifier neural recording applications. *IEEE J. Solid-State Circuits*, 38, 958–965.
- Wattanapanitch, W.; Fee, M.; Sarpeshkar, R. (2007). An Energy-Efficient Micropower Neural Recording Amplifier. *IEEE Trans. Biomed. Circuits Syst.*, 1, 136–147.
- Europractice (2025). Europractice IC Service, UMC Technologies, [on-line] <https://europractice-ic.com/>, accessed on 17th January 2025.